Laser Induced Breakdown Spectroscopy technique for detection of major elements in Particulate Matter from in-use Diesel engine passenger vehicles.

A dissertation submitted to the Department of Physics, Quaid-i- Azam University, Islamabad, in partial fulfillment of the requirement for the

degree of

Master of Philosophy in Physics

By

Mohsin Naeem

Registration No : 02182111037

Department of Physics

Quaid-i-Azam University Islamabad

2023

Dedicated To

My Beloved Parents

Teachers

Siblings

And Friends

ACKNOWLEDGMENT

All praises to Allah Almighty Who enabled me to achieve the milestone of my academic career. Countless Blessings of Allah be upon His most beloved and last Prophet; Hazrat Muhammad (S.A.W.W) who is the ultimate source of knowledge for the humanity.

First and foremost, I want to pay extreme gratitude to my research advisor Prof. Dr. Raheel Ali for his kind guidance and providing me the opportunity to do research work at Atomic and Molecular Spectroscopy Laboratory.

Moreover, I also feel obliged to thank my senior, Bilal Shafique (Ph.D. scholar) and Amir Fayyaz (Ph.D. scholar) for his continuous guidance and help during my entire research work.

Also many thanks to my labmates Akhtar Muhammad, Jamil who support me in all and guid me and cooperate with me in the tha lab.

I express my sincerest gratitude to my parents and siblings who supported and encouraged me at each step of my life.

Certificate

It is certified that the work contained in this thesis is carried out and completed under my supervision at the Atomic and Molecular Spectroscopy Laboratory, Department of Physics, Quaid-i-Azam University, Islamabad, Pakistan.

Submitted through

_____

Prof. Dr. Kashif Sabeeh

Chairman

Department of Physics,

Quaid-i-Azam University Islamabad, Pakistan

Supervised by

_____

Prof. Dr. Raheel Ali

Department of Physics,

Quaid-i-Azam University

Islamabad, Pakistan

Table of Contents

List of figures:

List of Tables:

Abstract

Successful applications of laser-induced breakdown spectroscopy (LIBS) for the elemental analysis of Particulate Matter from In-Use Diesel Engine Passenger Vehicles have been performed. A 532 nm Nd: YAG laser was used to create the plasma plume, and five channel HR 2000 spectrometer covering the wavelength range from 200-720 nm was used to record the spectra of the plasma plume. By using the online NIST database, the spectral lines are detected. The Boltzmann equation and the Stark broadening line profile were used to determine the electron temperature and number density before the quantitative analysis. The Boltzmann plot was drawn using spectral lines that were free of self-absorption, and the slope of the line was used to determine the electron temperature. The Stark broadening effect was employed to calculate the electron number density, and Voigt fitting was used to calculate the entire width at half maximum for the Stark broadened line. The quantitative analysis was performed using the calibration-free method which revealed that Ca and Fe are the major elements present in the Particulate matter sample. The concentration of other elements like Na, Li, Mg and Ni are also present in the Particulate matter sample.

Chapter 1

Introduction

1.1 Spectroscopy:

Around the turn of the 20th century, atomic and molecular physics started to get substantial scientific attention. Famous spectroscopists Balmer and Rydberg laid the groundwork for this important and expansive area of spectroscopy. Spectroscopy is the study of the interactions between light and matter. One of the best scientific methods for examining the natural world is this one. As a result, it shows both the intrinsic and extrinsic characteristics of matter. It involves exposing a substance to radiations in some way or gathering radiations emitted by an object, then studying those radiations to learn more about the substance's properties. Different kinds of radiation provide various kinds of information and are used to assess various substances. By means of analyzing the elements it contains and their concentrations, spectroscopy can use a material's unique identity to analyze it. It is typically not essential to touch the object being studied, despite the fact that it has shown us a lot about the physical processes that take place on Earth and the sun. At the same time, this incredible scientific method may provide details about atoms, molecules, and even the tiniest atom-forming particles. The atomic structure or a sample was initially studied qualitatively and quantitatively only using visible light. However, some sophisticated techniques for the spectroscopic investigation of materials have been established in our contemporary technological period of research. UV, X-rays, and infrared radiation are examples of electromagnetic radiation that can be used in this application.

1.1.2 Early history of spectroscopy:

Sir Isaac Newton is credited with developing spectroscopy when he discovered that white light breaks into seven different hues as it passes through a prism. The first spectrometer was

created in 1802 by William Wollaston, who used a lens to focus the sun's spectrum on a screen [1]. Wollaston discovered that colors were not evenly distributed and that there were eight missing patches of dark colors that appeared as bands in the Sun's spectrum [2]. Fraunhofer created the electroscope in 1814, and in 1817 he independently identified emission and absorption lines in the spectra of flames and the spectrum of the sun. Bunsen and Kirchhoff established the idea in 1859, according to which each element has a unique spectrum. Kirchhoff asserts that spectroscopy is governed by three laws:

➢ Hot gas under low pressure has the ability to emit "bright lines" or emission line spectra.

➢ Emission line spectrum is produced by any source of the continuous spectrum that may be seen through a cool, low-density gas.

➢ Incandescent solids, gases, or liquids under high pressure emit a continuous spectrum.

Due to the advent of quantum mechanics, significant progress in the theoretical aspects of spectroscopy was made in the 1920s and 1930s. Spectroscopy and quantum mechanics became quite similar as a result. The development of the laser created new opportunities in the study of spectroscopy. The development of numerous new spectroscopic techniques, in particular the dye laser innovation, has increased experiment precision.

1.1.3 Applications of Spectroscopy:

Spectroscopy has allowed both theoretical and experimental scientists to explore new areas of study. Here are some examples of spectroscopy's applications:

➢ Spectroscopy has allowed both theoretical and experimental scientists to explore new areas of study. Here are some examples of spectroscopy's applications.

➢ For a quantitative analysis of a sample to determine the amount of material in a sample, emission or absorption spectroscopy is highly helpful.

➢ The fields of biochemistry, biological research, and medicine all make extensive use of spectroscopy.

➢ Astrophysicists utilize the atomic spectrum to determine the physical properties of various objects. Spectroscopy is also useful in remote sensing.

➢ Atomic cooling, precise frequency measurements, and optical astronomy are some applications of contemporary spectroscopy.

➢ The majority of bodily fluid elemental studies involve spectroscopy [3].

1.1.4 Introduction to laser:

A method known as light amplification by stimulated emission of radiation (LASER) generates an electromagnetic radiation beam that is powerful, monochromatic, collimated, and coherent. In this method, an excited atom's emission is stimulated by a second photon, and the two photons move in the same direction to produce coherent, monochromatic light [3].

1.1.5 Multilevel laser system:

There are two energy levels in the basic understanding of laser activity. But the LASER mechanism should entail more than just two energy levels.

I. Three-Level Laser System:

There are three energy levels (E1, E2, and E3) in this system, one of which is a metastable condition. This facilitates the inversion of the population between the two energy levels. Electrons are pumped from E to E3, where they remain for a short amount of time before decaying back to E2, which is a called metastable state. This ensures population inversion between E and E2 and hence lasing action can be initiated.

II. Four-Level Laser System:

There are four different energy levels in this system, designated as E1, E2, E3, and E4, respectively. E4 provides temporary nonradioactive decay. Electrons from E are excited, and they fill up E4. They return to E3, a metastable state with a long lifetime relative to others, in a

remarkably brief period. Between E3 and E2, there is a population inversion, which causes the lasing activity.

1.2 Atomic Spectroscopy:

The study of emission or absorption spectra is referred to as spectroscopy. This is the greatest tool for determining the elements' composition. Atomic Emission Spectroscopy (AES), Atomic Absorption Spectroscopy (AAS), and Atomic Mass Spectroscopy (AMS) are three further subcategories of spectroscopy[4]. The study of emission and absorption spectra is the basic aspect of spectroscopy. Each element has a distinct electronic structure, which results in a distinct spectrum. The light's emission wavelengths are shown on the spectrum together with the number of counts and intensity for each individual length [5]. Calculations for the photon energy released or absorbed are as follows:

$$h\nu = E_2 - E_1 \qquad (1.1)$$

where E_2 & E_1 is the energy of the upper and lower level respectively.

1.2.1 Atomic Absorption Spectroscopy:

This process involves examining the sample's absorption spectra. According to the material's electrical structure, photons of particular wavelengths are absorbed in the sample as continuous radiation passes over it [6]. When the transmitted light's spectrum is examined, the elements can be identified.

1.2.2 Atomic Emission Spectroscopy:

With this method, we examine a sample's optical emission spectrum. With the use of a light source or electrical discharge, the sample is initially excited to higher energy levels. Promotion to higher energy levels occurs for atoms. They eventually decay to lower energy levels (stable states), when they release the absorbed energy as photons. The electrical structure of the elements determines the

wavelengths of the photons that are released. An optical spectrometer is used to record the photons' wavelengths. These wavelengths could be in the infrared, visible, or even X-ray spectrum. We can obtain an optical fingerprint of the sample's elements constituents by examining these wavelengths. Since each sample has a different fingerprint, identification is carried out [7].

1.2.3 Atomic Mass Spectroscopy:

The study of the mass spectrum of a sample is known as mass spectroscopy. Elements are subjected to an external electric and magnetic field. These fields separate the elements depending on their charge-to-mass ratios. Electric field accelerates the elements and magnetic field give them circular paths. These paths follow the relation:

$$r = \frac{mv}{qb} \tag{1.2}$$

where r is the circumference of the circle, q is the charge on the element, v is the speed, and B is the magnetic field that is being applied. According to the relationship above, the pathways taken by heavy and lighter elements will differ [8]. This spectroscopy is used to separate the isotopes of various elements. Isotopes take distinct pathways in the area of the electric and magnetic fields because they have different masses. As a result, they are split.

1.3 Laser-Induced Breakdown Spectroscopy:

The technique known as Laser Induced Breakdown Spectroscopy (LIBS) involves examining the optical emission spectrum [9]. This is a great method that may be used to study the substance in all three of its states (solid, liquid, and gas). Pre-sample preparation is not required [10]. In comparison to previous spectroscopy approaches, this method is quicker, more effective, and less expensive [11]. There are uses for LIBS in practically every area of science. Recent developments in LIBS have made it possible to analyze distant targets remotely. This aids in the analysis of potentially explosive and dangerous materials. Space exploration has become simpler as a result [12]. In some circumstances, LIBS may have some restrictions. The amount of laser power being employed is frequently a restriction on analysis. The laser energy from a single shot of the laser may not be sufficient to excite the target sample [13]. This may prevent the

sample from being stimulated and atomized. Therefore, we must choose the laser's energy wisely. The LIBS spectroscopy is also constrained by the sample's environment. Despite all of these drawbacks, researchers frequently employ this technique. In conclusion, LIBS has demonstrated to be an incredibly promising approach for a variety of materials.

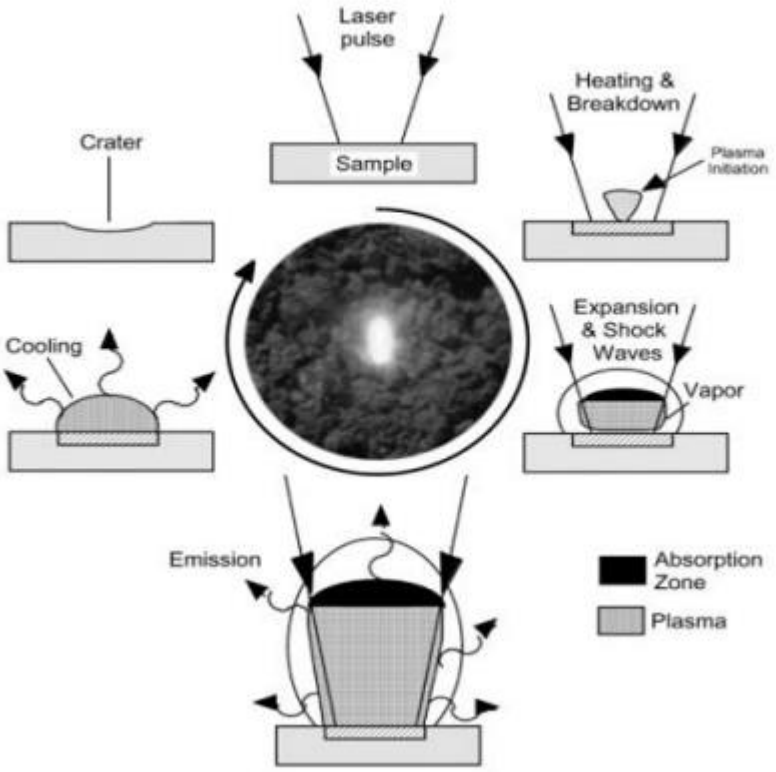

Figure 1: Plasma evolves through several transient phases between its initiation and decay

1.3.1 Basic Principle of LIBS:

The target sample's excitation and de-excitation form the foundation of LIBS's operation. A laser is used as an excitation source to stimulate the target. The material is atomized by a strong laser beam that is concentrated on a small region of the target. On the target sample, plasma is created. Photons are released by the plasma when it is de-excited. Since each element emits radiation at distinctive frequencies, an optical spectrometer is used to record these radiations. This spectrometer collects every wavelength that the plasma emits, producing a spectrum of every radiation. Based on the wavelengths

that the sample emits, this spectrum can be used to determine the elements that are present in the sample.

1.3.2 Target Ablation:

There could be a variety of responses occurring on the target's surface while the laser beam is concentrated on a small area of the target. These reactions might be influenced by several elements like laser power, pulse duration, spot size, and sample type. Some significant phenomena are characterized as follows [14]:

1. 1. The energy of the laser light is transmitted to the atoms by collisions, raising the sample's temperature. This method turns laser energy into thermal energy. Vibrations in the lattice transport the thermal energy to the sample matrix. The target melts and vaporizes more quickly as the sample's temperature rises. Photo-thermal ablation is the term used to describe this mechanism [15].

2. A few atoms might absorb some energy and become excited. Electrons are capable of jumping from lower energy levels to excited states. This occurs when the laser energy is strong enough to ionize the sample, such as using a femtosecond laser. Even most of the time, the atoms are ionized as a result of the absorption of energy, and the resulting electron jumps to higher states. This is called photochemical ablation [16].

3. There is a third method of ablation, which combines the first two methods. Free electrons are generated during the photochemical reaction. The laser energy is delivered to the matrix by these electrons as they move through it photothermally. The material is vaporized and ablated as a result [17].

1.3.3 Post-Ablation Processes:

When a laser is directed at a target, the interaction between the laser and matter is extremely complicated. There are lots of complicated events that are taking place. The laser's beam's leading edge

shines on the surface and releases energy into the atoms there. Material is ablated when the laser energy per shot is equal to (or higher than) the threshold energy necessary for ablation [18].

After the target has been ablated, the majority of the material is transformed into vapors, which are primarily composed of neutral atoms and electrons. Now, the material that was previously ablated engages with the laser beam's trailing edge. These electrons and vapors absorb the laser energy and get ionized. Around the target's surface, a plasma with a high degree of ionization is produced.

1.4 Plasma

The fourth state of matter, known as plasma, can be generally described as a highly ionized gas made up of ions and electrons. The most complete and correct description of plasma, aside from the one provided above, is given in the following sentence:

"A quasi-neutral gas of charged and neutral particles that exhibits a collective behavior is called plasma"[19].

Plasma is made up of ions, electrons, and neutral atoms; in some areas of the plasma, the concentration of charged particles, such as ions or electrons, may be higher than in other areas, indicating the plasma's charge character, but in reality, the number density of ions and electrons in the plasma is roughly equal ($n_i \approx n_e$), indicating the plasma's overall neutral nature. To put it another way, an observer inside the plasma will find themselves inside a cluster of charged particles, whereas an observer outside the plasma will regard the plasma as a whole as neutral. Plasma has what is referred to as quasi-neutral behavior. Another crucial characteristic of plasma that is mentioned in the definition is collective behavior. A little amount of the plasma can be perturbed by an electric field, magnetic field, or other force, and the entire plasma will react to the perturbation. This property is called collective behavior. A further crucial characteristic of plasma is conductance; as an ionized gas with free charge carriers, plasma excels as a conductor.

1.4.1 Plasma expansion

At the early stages of the plasma formation, it is highly ionized and possess high temperatures. Most of the time, the plasma temperature ranges to about 100.000 K. Plasma emits radiation in the continuous range at such high temperatures. The detection of composition using this spectrum is not particularly effective [20]. Plasma eventually grows and cools down. The temperature drops to 4,000–

2,000 K. Plasma is currently emitting the distinctive frequencies of the elements in the system [21]. An optical spectrometer is used to record these radiations. This is the basis principle of LIBS technique.

1.4.2 Plasma Parameters:

Neither any ionized gas can be referred to be plasma. A gas will always have some level of ionization. A gas has to meet the following three prerequisites or characteristics [22]:

1. $\lambda_D << L$

2. $N_D >> 1$

3. $\omega\tau >> 1$

where N_D represents to the number of particles in the Debye sphere which can be written as:

$$N_D = n \frac{4}{3} \pi \lambda_D^3 \qquad (1.3)$$

1. The Debye length λ_D should be substantially less than the plasma container's dimensions. This requirement makes sure that when an external potential source is introduced into the plasma, it is shielded out in a zone that is smaller than the chamber's size.

2. The symbol N_D is the amount of particles in the Debye sphere. To ensure the collective behavior of the plasma species, this criterion specifies that there should be a large number of particles in the Debye sphere.

3. The plasma oscillation frequency is ω, and the mean relaxation period in between collisions with neutral atoms is denoted by the symbol τ. This need makes it necessary for electromagnetic forces to regulate plasma motions rather than conventional hydrodynamic forces.

1.5 Plasma Characterization in LIBS:

The most important aspect of plasma spectroscopy approaches is plasma characterization because emission lines provide sufficient information about LIBS. Number density and plasma temperature are both provided via plasma characterization. This section provides a quick explanation of how number density and plasma temperature are calculated.

1.5.1 Assumptions in the Plasma Characterization:

There are several limitations placed on the plasma throughout the process of characterization. First, local thermodynamic equilibrium is necessary for the investigation of plasma dynamics and the evolution of the various plasma states. The reverse deactivation process balances excitation mechanisms, and thermodynamic equilibrium assures that all processes in plasma dynamics are governed by a single temperature. Local thermodynamic equilibrium and optically thin spectral line emission are the two main assumptions that need to be verified while doing the plasma characterization in the laser induced breakdown spectroscopy.

1.5.2 Local Thermodynamic Equilibrium LTE:

Two of the most well-known equilibrium equations must be applied in order to determine plasma temperature. The first Boltzmann equation, which models population energy level as a function of temperature [25] i.e.

$$\frac{N_j^Z}{N^Z} = g_j e^{-\frac{E_j^Z}{kT}} \tag{1.4}$$

Superscript "z" in this equation represents the ionization stage (z=0 for neutral and z=1 for singly ionized ions), N^Z represents the number density, E_j^Z represents the level's energy, g_j represents the level's degeneracy, and k represents the Boltzmann constant. The Saha: Boltzmann equation is the second equation, and it describes the densities of the ionization species that follow as a function of temperature [23] i.e:

$$\frac{N_e N_z}{N^{z-1}} = \frac{2U^Z(T)}{U^{Z-1}(T)} \left(\frac{2\pi mkT}{h^2}\right)^{\frac{3}{2}} e^{-\frac{E_\infty^{Z-1} - \Delta E_\infty^{Z-1}}{kT}} \quad (1.5)$$

where h is plank's constant, $U^Z(T)$ is the partition function, m is the mass of the electron, and N_e is the electron number density. E_∞^{Z-1} is the ionization energy of the Z-1 species, The reliability of local thermodynamics The use of these two equations requires equilibrium, which is a necessary condition. All species (neutral, ions, and electrons) are subjected to the same temperature in a local thermodynamic equilibrium. It is simple to use statistical mechanics to examine the dynamics of the entire system.

Kirchhoff's law of radiation is also corroborated by LTE [24] i.e:

$$\frac{\mathcal{E}_\lambda(\lambda)}{k\prime(\lambda)} = B_\lambda(\lambda, T) \quad (1.6)$$

where $B_\lambda(\lambda, T)$ is the blackbody radiation's intensity at temperature T.

The radiative processes should be driven by electron collisions to maintain local thermodynamic equilibrium (LTE). A minimum electron number density of around 101 cm is needed for this scenario. McWhirter [25] proposed a criterion that guarantees LTE for a threshold electron number density value. i.e:

$$N_e \geq 1.6 \times 10^{12}\ T^{\frac{1}{2}} (\Delta E)^3\ \text{cm}^{-3} \quad (1.7)$$

where T (K) is the excitation temperature and ΔE (eV) is the greatest energy gap between the transition levels.

1.5.3 Optically thin spectral line emission:

The state of the optically thin spectral line emission is also taken into consideration when calculating the plasma parameters (excitation temperature and electron number density). The emission lines must be optically narrow in order for the Stark broadening effect to be used to calculate the electron number density and to determine the plasma temperature using the Boltzmann and Saha-Boltzmann equations. This indicates that the lines do not exhibit self-absorption, are not saturated, and do not exhibit distorted areas or widths [26]. Failure to achieve this condition will result in inaccurate estimations of the electron number density and plasma temperature. The relative strength of the measured emission lines can be used to confirm the existence of optically thin spectral line emission. For Calculating the intensity ratio is as follows:

$$\frac{I_1}{I_2} = \frac{A_1 g_1 \lambda_2}{A_2 g_2 \lambda_1} \, e^{-\left(\frac{E_2 - E_1}{kt}\right)} \tag{1.8}$$

Calculating the non-resonance spectral line's line width is another approach to make sure of this. The lines are visually thin if their width is constant across all axial positions [15].

Calculation of Electron Number Density:

1.5.4 Stark Effect:

A broadening of the emission line profile brought on by the presence of an electric field is known as the Stark broadening or Stark effect. The atom that is radiating interacts with the electrons and ions that are already present in the area. The line profile is impacted by the electric field created by these electrons and ions. The Stark effect causes line broadening for hydrogen and hydrogen-like atoms, as shown by [27].

$$n_e \text{ (cm}^{-3}\text{)} = \left(\frac{\Delta\lambda_{FWHM}^{S}}{2\omega_s(\lambda, T_e)}\right) N_r \tag{1.9}$$

where N_r is the reference electron density, which is on the order of 10^{16} cm^{-3}, $\Delta\lambda_{FWHM}^{S}$ is the full width at the half maximum, ω_s is the Stark broadening parameter, and n_e (cm^{-3}) is the electron density.

Theoretical calculations on the broadening of the spectral line caused by the quadratic Stark Effect for atoms with two or more electrons are provided by [28].

$$\Delta\lambda_s \approx 2[1+1.75A(1-0.75R)]w\frac{N_e}{N_e^{ref}} \quad (1.10)$$

The electron-impact half width is denoted by the symbol w, the ion broadening parameter by the letter A, the electron number density by the letter N, and the reference electron number density by the letter N_e^{ref}, which is roughly of the order of 10^{16} or 10^{17} cm^{-3}. The lines chosen for the number density computation should be optically thin and interference-free. The calculation of the electron number density contains inaccuracy due to the measurement of the Stark width.

1.5.5 Calculation of Electron Temperature:

Calculations of the excitation temperature make up the second aspect of plasma characterization. The elemental composition of the sample can be incorrectly determined if the plasma temperature is not estimated appropriately, which is necessary. The Boltzmann equation below can be used to compute the plasma temperature [29] i.e:

$$\ln\left(\frac{I_{ik}\lambda}{A_{ki}g_k}\right) = -\frac{1}{kt}E_k + ln\left(\frac{hcN^Z}{4\pi U^Z(T)}\right) \quad (1.11)$$

Where I_{ik} be the intensity of the transition line joining energy levels i and k, λ is the wavelength, A_{ki} and g_k are the transition probability and statistical weight of the upper level, E_k is the energy of the upper

level and U^Z(T) is the partition function, that depends on plasma temperature. A straight line results from plotting the LHS of the Boltzmann equation as a function of E_k.From the equation above the slope is equal to $-\frac{1}{kT}$. We can find the plasma temperature by calculating the slope of line. It is important to choose the spectral lines for plotting carefully. Self-absorption should not occur in the lines, and the energy in the upper levels should be substantial. Self-absorption in the spectral lines may result in incorrect temperature estimate.

1.5.6 Quantitative Analysis through Calibration Free LIBS:

There are two distinct methods used in LIBS to analyse the elemental configuration. The calibration curve method is one, and the calibration free method is another [30]. Using Calibration Free LIBS is an easy and effective technique. The composition of the sample can be approximated using the plasma temperature and number density, which are calculated. One-line calibration free approach is typically performed. Atomic concentration is calculated using the Boltzmann equation and is provided as:

$$FC^Z = I_k \frac{U^Z(T)}{A_{ki} g_k} e^{\left(\frac{E_k}{kT}\right)} \tag{1.12}$$

where $A_{ki,}$ g_k and E_k denote for the transition probability, upper level statistical weight, and upper level energy, accordingly, and C^Z is the concentration of the neutral species, the intensity of the spectral line, U^Z (T) is the partition function at plasma temperature, and. F is a factor that affects plasma length [31].

$$F = \frac{L}{4\pi} \tag{1.13}$$

Where L is the plasma length in the above equation. For a constant spectral system, this factor is constant. Therefore, the concentration of the neutral elements can be determined using an optically narrow spectral line of an element using the Boltzmann equation stated above.

The Saha-Boltzmann equation is utilized to determine the concentration of ionized species [32].

$$\frac{C^{Z+1}}{C^{Z}} = \frac{(2m_e kT)^{\frac{3}{2}}}{n_e h^3} \frac{2U_{Z+1}}{U_Z} e^{-\frac{E_{ion}}{kT}} \quad (1.14)$$

where C^{Z+1} is the ionized species concentration, U_{Z+1} is its partition function, and E_{ion} is the energy of ionization. The formula for calculating each element's percentage concentration is [33]:

$$\%C_{element} = (C_{element}/C_{sum\ of\ elements}) \times 100 \quad (1.15)$$

1.6 Line broadening:

Line broadening at specific wavelengths or frequencies affects the capacity to extract information from the spectrum both numerically and qualitatively. A spectroscopic shift's line form and width can be determined using the broadening mechanics of the starting and final levels. Line shape is further impacted by additional homogenous broadening mechanisms as Stark, Pressure, and Natural broadening. Through the use of these homogenous broadening methods, Lorentzian form lines are produced. Gaussian line form results from inhomogeneous broadening, such as Doppler broadening. It means that both homogeneous and inhomogeneous mechanisms are affected by the naturally broadening. Below are a few of the physical mechanisms.

1.6.1 Natural broadening:

The most fundamental line broadening is that which results from an isolated atom (an atom with no external perturbation, such as an electric field, pressure, or temperature). Heisenberg's principle can be used to explain this broadening phenomenon as follows:

$$\Delta E \Delta t \approx \hbar \quad (1.16)$$

This implies,

$$\Delta v = \frac{1}{2\pi\Delta t} \tag{1.17}$$

In a certain energy level, an electron has a specific lifetime. As electron's energy level uncertainty can be derived from how long it spends in that level, as seen in the equation above (1.17).

Since short lifetime levels have a significant degree of energy level uncertainty, the spectrum tends to broaden. A spectrum with a higher level of uncertainty has a wider range of frequencies. When compared to other broadening methods, the effect of the natural broadening mechanism is typically extremely small.

1.6.2 Pressure broadening:

High density materials are mostly impacted by the broadening. This broadening mechanism occurs when gas atoms undergo transition under high pressure. This widening results from the high pressure collision of gas atoms. Collision broadening is another name for pressure broadening. The spectral lines' pressure broadening form is Lorentzian. In a nutshell, we may say that the interaction of radiating atoms with adjacent atoms is what causes the frequency to broaden.

1.6.3 Stark broadening:

The homogeneous broadening mechanisms' Stark broadening, which is the most effective, the system's electron-radiating atom interactions are the main cause of the Stark broadening. This definition demonstrates that it is strongly temperature sensitive and directly reliant on concentration or electron number density around the emitting species. Stark broadening can be used to measure electron number density (N.). The equation for calculating the full width at half maximum (FWHM) of a spectral line (i.e. Stark broadening) is shown below.

$$\Delta\lambda_{1/2} = 2\omega\left(\frac{N_e}{10^{16}}\right) + 3.5A\omega\left(\frac{N_e}{10^{16}}\right)^{\frac{5}{4}}\left[1 - \frac{3}{4}N_D^{-\frac{1}{3}}\right] \tag{1.18}$$

Where

ω stands for the impact width of an electron.

A represent ion broadening parameter.

N_e is the density of electrons.

In the Debye sphere, N_D stands for the number of particles.

The first term in the equation above depicts the result of an interaction between electrons, and the second component in the equation represents an interaction between atoms and ions. Normally, the second term in this equation is discounted because it rarely has any significant effects. Due to Stark broadening, the spectral line has a Lorentzian structure.

$$\lambda_{1/2} = 2\omega\left(\frac{N_e}{10^{16}}\right) \tag{1.19}$$

1.6.4 Doppler Broadening:

This broadening was attributed to the area around the radiating species. Doppler broadening is a term used to describe the frequency shift caused by the relative motion of the source and observer. Given that Doppler broadening is an inhomogeneous mechanism for line broadening, its line shape is Gaussian. Since atoms are always moving randomly, we can regulate the thermal motion of the atoms by adjusting the system's temperature. When the source (atom) moves away from the observer (detector), a little shift in frequency is achieved in the form of a red shift, and when the source (atom) moves toward the observer (detector), a slightly bigger shift in frequency is acquired in the form of a blue shift. Consequently, a change in the frequency of observed photons will take place as a result of thermal disturbance of atoms.

$$\Delta\lambda_D = \lambda_0\sqrt{\frac{8kTln2}{m_A c^2}} \tag{1.20}$$

The given equation illustrates a shift brought on by relative wavelength motion, which depends on the system's temperature.

Where:

In a spectral line (m), the central wavelength is represented by λ_0

T represent the absolute temperature (K)

m_A represent the atomic mass (Kg)

k represent the Boltzmann constant (J/K)

C represent the speed of light (m/s)

Chapter 2

Experimental Setup

2.1 Setup for LIBS Experiments:

In fig, a schematic for the LIBS setup to analyze the particulate matter sample is shown. In our experiment, a 10Hz repetition rate and a 5ns pulse duration Nd: YAG Q- switched laser is used as to light the source. This laser can produce 200mJ of energy at a wavelength of 532nm and 400mJ of energy at a wavelength of 1064nm. By adjusting the Q-switch delay in relation to the flash lamp source, the pulse energy can be changed. A joule meter can be used to measure laser or pulse energy [34]. With the help of a 20 cm convex lens, the laser beam is focused on the sample of particulate matter sample. In order to rotate the sample consistently and avoid the non-uniform pits in the Particulate matter sample, a 3-D sample stage is utilized to place the sample in front of the laser beam. To eliminate the possibility of any breakdown in the air surrounding the sample, the particulate matter sample is positioned somewhat away from the center of focus and toward the focusing lens. Seven single laser shots were captured, each with a varied pulse delay that altered the laser's pulse energy. A fiber optic set at a right angle to the path of the laser beam is used to collect the electromagnetic radiation that the plasma plume emits. This fiber optic's field of view ranges from 0 to 45 degrees, and its core diameter is 600 µm. This fiber optic was connected to a detecting device (LIBS 2000) to capture the spectrum of the plasma emission. The detecting system includes five distinct spectrometers, each of which is designed to trace the emission spectra of the plasma over a particular frequency band. Each spectrometer has an optical resolution of up to 0.06 nm and a silt width of 5 µm. Each of these spectrometers has a 2048-element linear CCD array and covers a wavelength range of 200 to 700 nm. The Nd: YAG Laser was operated by the detecting system LIBS2000, which was linked with a Q-switched Nd: YAG Laser to capture the spectrum. The connection between the laser and detecting system was made using a pulse generator (SRG DG 535) or a five channel digital delay.

The software OOILIBS2000 (Ocean Optics Inc. Laser Induce Breakdown Spectroscopy) was used for both correcting the emission spectra by removing the dark signals and for controlling the energy of the laser beam. Using the DH-2000 standard light source, the manufacturer calibrated each of the installed spectrometers in the LIBS2000 detection system. The computer programme OOLIBS was used to record the plasma's spectrum for further examination.

Schematic diagram of LIBS.

The basics of the experiment are depicted in the figure 2. Below is a detailed note on each instrument installed in the LIBS experimental setup.

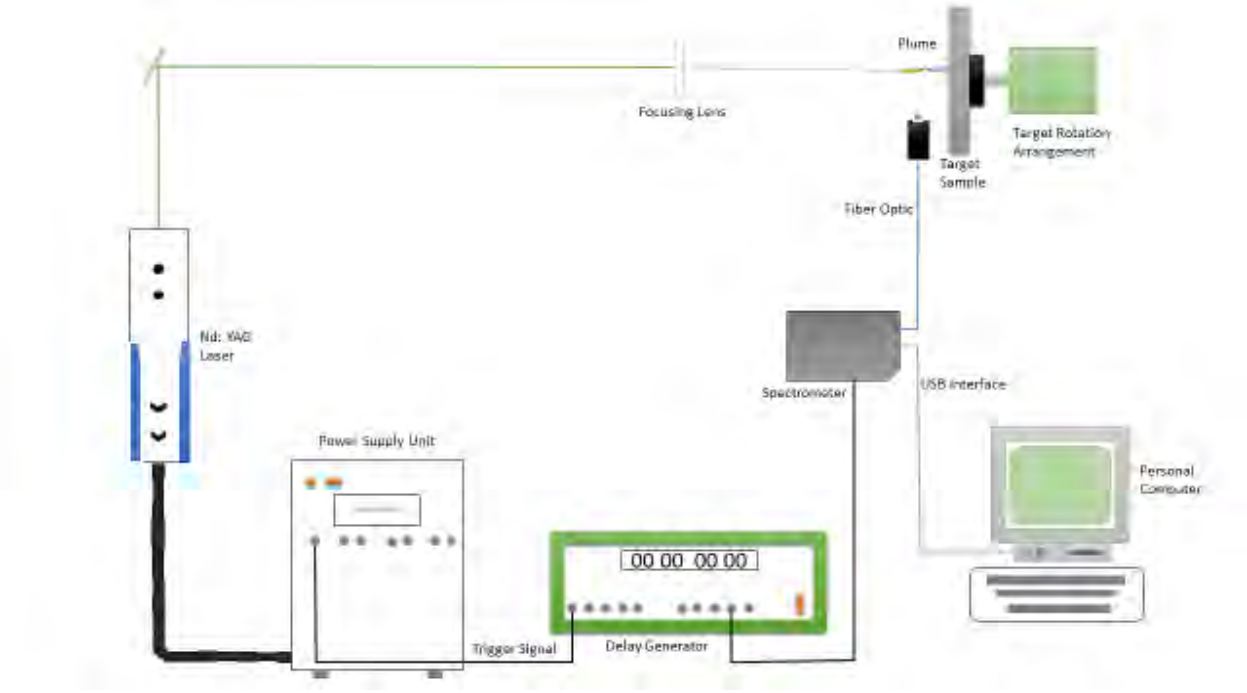

Figure 2: The figure shows the schematic diagram of pulsed LIBS analysis setup

Here is a list of the equipment's we utilized in our experiment:

- Q-switched Nd: YAG Laser
- Focusing lens
- Detection system (LIBS 2000)
- Triggering device
- Fiber optic cable
- Personal Computer

2.2 Nd: YAG Laser:

The Nd: YAG laser is the most used solid state laser, is utilized in the LIBS experiments and numerous other experiments. The laser's active lasing medium is a Neodymium-doped Yttrium Aluminum Garnet crystal. Neodymium, a dopant, has a crucial rule for altering the crystal's optical characteristics. Because the host (YAG) and active ingredient (Neodymium) have the same size, Neodymium ions modify the host (YAG) in the crystal. The positively charged Neodymium ions Nd+3 are optically pumped using the flash lamp as a source. The four-level Nd: YAG system's energy level diagram is shown in the figure 3.

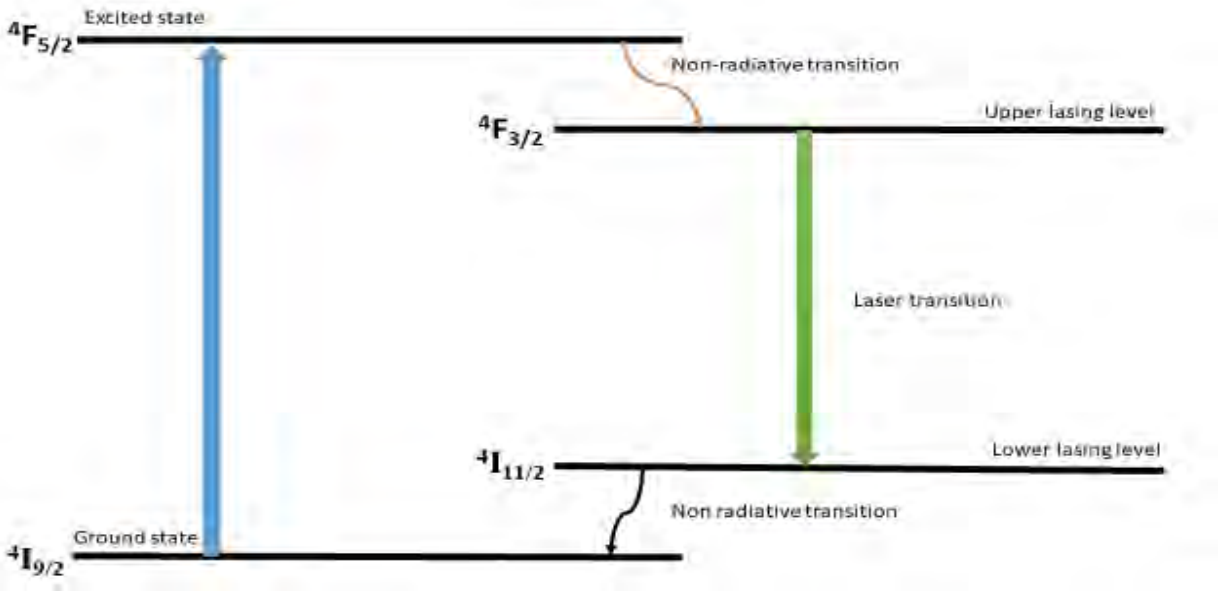

Figure 3: Energy level diagram of Nd: YAG crystal

Neodymium's ground state atom has the electronic configuration (Xe)$4f^4 6s^2$. The J values for ^{4}I with L=6 and S=3/2 are 15/2, 13/2, 11/2, and 9/2, respectively, in the Russel Sounder approximation. This means that a lower value of J will have the lowest energy. As we can see from the diagram above, the transition between the states $^4F_{3/2}$ and $^4 1_{11/2}$ is generally necessary for the generation of a laser beam. The Probability of other transitions also increases with the splitting of energy levels in to their part. The dominant wavelengths at 300 K, which is room temperature, and 77 K, which is lower temperature, are 1064.8 nm and 1061.2 nm, respectively. The slight movement in the levels of $^4I_{11\backslash 2}$ and $^4F_{3/2}$ is what causes the variation in wavelengths.

2.3 Detection System (LIBS 2000):

Five HD 2000 type spectrometers of high resolution make up the US 2000 detection system. These spectrometers have a resolution of roughly 0.06 nm. These spectrometers, which have either 2400 or 1800 lines per millimeter gratings, cover the whole optical range. Every HR 2000 spectrometer's database was used in the software's layout. Through a data cable, the computer system and detecting system are linked so that the computer may run the OOLIBS software and acquire spectral images. When we shine a laser beam in pulse mode on a sample that is being studied, photons from the laser beam transfer their energy to the sample's atoms and become excited. After a period of time (roughly a few hundred nanoseconds), these excited atoms become de-excited along with the emission of radiations, which is what the spectrum on the computer screen represents. To connect the detected radiations to the emitting radiations, fiber optics are utilized. The detecting device on the grating captures the radiations that are released and sends the data to the programme on the computer as digital signals. It is really helpful to have the software OOILIBS available so that we may capture any form of optical spectrum. The software's digital library has the ability to regulate every setting, gather data, and display the optical spectrum.

The parameters of the high-resolution spectrometers used in the experiment's detection system are displayed in the table 1.

Specification of different HR 2000 used in LIBS 2000+ spectrometer			
Model	**Grating (lines/mm)**	**Region**	**Band width**
LIBS HR 1	2400	Ultraviolet	200-301 nm
LIBS HR 2	2400	Ultraviolet	296-391 nm
LIBS HR 3	1800	Visible	386-513 nm
LIBS HR 4	1800	Visible	509-623 nm
LIBS HR 5	1800	Visible	619-720 nm

Table 1 : Specification table for the LIBS detection system

2.4 HR 2000 High Resolution Spectrometer:

Resolution capabilities of a fiber optic HR 2000 spectrometer can reach 0.065nm FWHM. The HR 2000 spectrometer is used to measure the high-resolution lines given off by atoms or gases.

Any spectrometer's resolution is dependent on its grating and entry slit width. The HR 2000 spectrometer operated without the need for an external power source. Data cable is used to supply power to the detecting system from the computer system. When a laser beam contacts a sample, it creates a plasma plume of the sample in which the atoms are excited. After the atoms have been de-excited, they release radiations that are collected by the detection system and sent to the computer system in the form of an electrical signal for further processing. The data is presented and analyzed by the software OOILIBS. In the figure below, an optical worktable for the HR 2000 spectrometer is shown in figure 4.

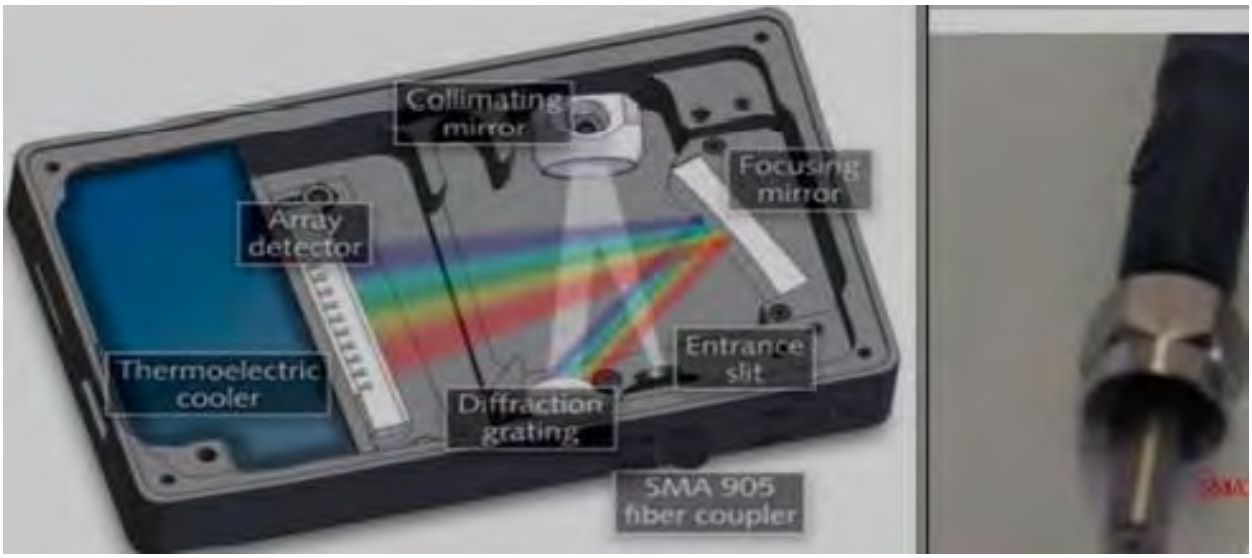

Figure 4 : Schematic diagram of the HR 2000 High resolution spectrometer

2.4.1 SMA Connector:

An optical bench is connected to fiber optic via a SMA connector, which is placed at the spectrometer's entrance slit.

2.4.2 Slit:

The radiations enter the optical counter through the slit after passing through the SMA connector, which acts as a slit. The amount of radiation that enters the system is directly influenced by the slit's width. Our LIBS experiment used slits that were 5µm wide.

2.4.3 Absorbing Filter:

The SMA connector and this filter device are permanently attached to each other. The filter's job is to limit the wavelengths of light that enter the detection system by blocking some specific wavelengths that fall outside the detection range of the installed spectrometers and allowing passage of wavelengths that fall inside that range.

2.4.4 Collimating mirror:

The purpose of a collimating mirror is to reflect incident radiations back toward a grating system from an entrance slit. Collinear rays are reflected from the incident radiation by the collimating mirror.

2.4.5 Grating:

Collinear beam diffracts after passing through grating system and after collimating mirror reflection. The grating (lines/mm) of each spectrometer in the detecting system varies from 1800 to 2400 and each has its unique specifications. The grating arrangement virtually completely and accurately covers the entire light spectrum.

2.4.6 Focusing mirror:

The focusing mirror's job is to point the spectrum in the direction of the detector.

2.4.7 Detector collection lens:

To capture the largest possible portion of the radiation spectrum that has been gathered, a large diameter cylindrical lens is required. In principle, this lens directs radiation in the proper direction and concentrates it on the detector.

2.4.8 CCD Detector:

The CCD detector is the most crucial and significant component of the detection system. Each pixel in the detecting system responds solely to a particular wavelength when radiation strikes the detector, which is constructed of a 2048-element linear CCD array.

Chapter 3

Results and Discussion:

An Nd:YAG laser is utilized as the energy source for plasma formation in order to investigate the emission emanating from the laser-produced plasma on the surface of the Particulate matter sample. The Q-switched Nd:YAG utilized in our experiment had a frequency of 10 Hz and operated at a wavelength of 532 nm through second harmonic generation (SHG) at 532 nm and time delay 10μs at laser energy of 34.4 mJ. A convex lens with a 10 cm focal length was utilized to concentrate the pulsed laser beam on the Particulate matter sample By using the laser as externally triggered. The target surface's distance from the focusing lens is adjustable using a mobile microscope with a convex lens installed. The fiber optic is mounted on an adjustable stage that moves towards the plasma point. Through the fiber optic, the HR2000 spectrometer was connected to the laser-ablated plasma emission. The computer has received the recorded data from the spectrometer along with the lines of emission from the laser-induced plasma. The emission lines were captured at a right angle to the incoming laser beam and come from the DPM sample plasma that the laser beam has created.

3.1 Particulate Matter Collection and Sample Preparation:

DPM sample was obtained from miscellaneous in-use diesel-engine passenger vehicle of diverse type and model from major brand car producer. DPM sample was collected from diesel-powered passenger vehicle that was in used and came from well-known automaker. Vehicle from production model that is often seen on public roads was chosen for the sample collection. Neither prototype vehicle nor test engine was utilized. It is important to note that the technical setup and characteristics of specific vehicle has not been the focus of these investigations. Additionally, we haven't measured the mineral composition of engine intake air or the particles adhered due to the air filter of the vehicle, thus the air pollution hasn't been taken into account. Because vehicle has been operating in many environments throughout their live, it would be difficult to analyse both situations. Diesel particulate matter has been removed from the passenger vehicle tailpipe end portion, or from the area right after

the Diesel Particulate Filter (DPF), Diesel Oxidation Catalyst (DOC), or catalytic converter, if any of these devices have been used. We carefully extracted from the upper portion of the stored residual deposits of particulate matter from the tailpipe wall for this purpose. Vehicle was chosen at random, with no preferred manufacturer. Sample was analysed using the LIBS technique. The results from this study come from DPM matrix in terms of the LIBS spectrum. The goal is to use laser induced breakdown spectroscopy to qualitatively and quantitatively describe the elements that make up these matrix. Analysis of the major spectral lines that are most prominent in the ultraviolet, visible, and infrared optical emission spectrum from diesel particulate matter is given specific attention. The collected diesel-engine exhaust particle was mechanically compressed into solid pellet in a flat disc form. After that, LIBS performed an analysis on the DPM sample without further preparation.

3.2 Spectrum Analysis:

The classified spectrums of the particulate particles is shown in Figures 5 - 7. Thus, Figure-8 displays the complete spectrum in the wavelength range of 235-715 nm, which displays both strong and weak emission lines, consisting of the elements lithium (Li), hydrogen (H), sodium (Na), calcium (Ca), iron (Fe), and carbon (C)), as well as a multiplet cluster of singly ionised magnesium (Mg II), because of the $3p^2P_{1/2,3/2} \rightarrow 3S\ ^2S_{1/2}$ and $3d\ ^2D_{3/2,5/2} \rightarrow 3p\ ^2P_{1/2,3/2}$ Transitions. The spectrum was separated into sections in order to have a clear understanding of the spectrum due to the large number of spectral lines. In the Table 1.2 The wavelength of all the emission lines of the emission spectrum of the Particulate matter sample classified, which shows that Ca and Fe has the major lines in the spectrum. Each of these lines was identified from proper checking while using the NIST database.

The presence of Ca, Fe, Na, Cu, Ni, Li, and Mg is confirmed by spectral lines. Na, Li, and Cu are trace elements, while Ni is a minor chemical element. However, the intensity and number of lines for Ca, Na, Mg, and Fe Show that these are the major elements present in the sample.

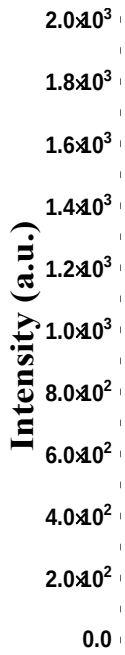

Figure 5 : Classified emission spectrum of DPM covering the spectral range for 235-365 nm at energy of 34.5 mJ

Figure 6 : Classified emission spectrum of DPM covering the spectral range for 355-465 nm at energy of 34.4 mJ

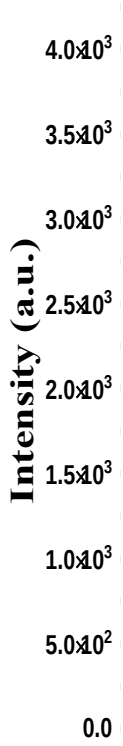

Figure 7 : Classified emission spectrum of DPM covering the spectral range for 365-715 nm at energy of 34.4 mJ

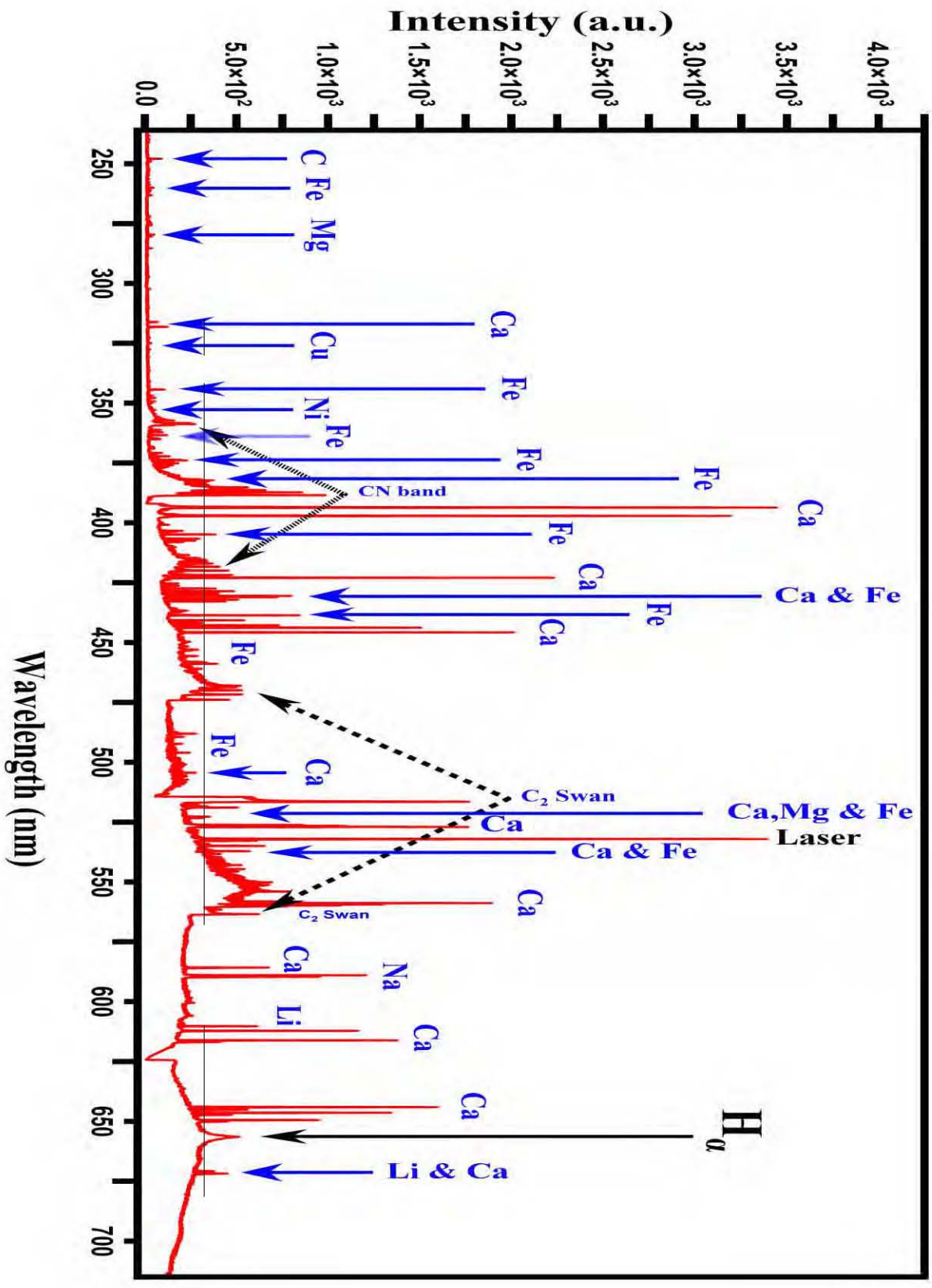

Figure 8 : Classified emission spectrum of DPM covering the spectral range for 235-715 nm at energy of 34.4 mJ

Elements	Wavelengths
Hydrogen(H)	656.46 (H_α)
Carbon(C)	247.91
Sodium(Na I)	588.94, 589.54
Lithium (Li I)	670.78, 610.21
Magnesium (Mg I)	285.28, 517.25, 518.36,
Magnesium (Mg II)	279.59, 280.34
Calcium (Ca I)	316.08, 318.12, 397.85, 422.90, 428.52, 429.17, 429.66, 430.13, 430.48, 431.00, 442.76, 443.74, 445.72, 339.57, 396.85, 441.73, 504.37, 518.36, 518.86, 526.18, 526.54, 527.00, 534.92, 558.81, 558.13, 559.37, 559.78, 585.70, 616.14, 616.86, 644.01, 645.08, 646.34, 647.25, 671.77
Calcium (Ca II)	393.57, 396.85
Iron (Fe I)	344.59, 344.26, 259.99, 361.07, 362.06, 363.31, 364.64, 364.97, 427.40, 425.28, 425.30, 375.99, 376.55, 376.88, 368.19, 368.94, 370.76, 371.11, 372.17, 372.43, 373.87, 372.99, 376.55, 381.74, 382.19, 400.74, 403.30, 404.81, 406.58, 407.38, 408.00, 438.58, 522.70, 523.27
Copper (Cu I)	324.94, 327.58
Nickel (Ni I)	352.81, 352.33, 351.59, 341.51

Table 2 : Singnificant number of emission lines were found in the emission spectrum of the DPM

3.3 Emission of the CN Violet and C_2 Swan System:

Figure-9 illustrates the molecular emission structure of the CN violet band and C_2 swan band in the emission spectra of Particulate matter, which range in wavelength from 384 to 421 nm for CN violet band and from 450 to 700 C_2 swan band. In diatomic molecule's molecular optical emission in the CN violet system is related to radiative transitions from the electronic state for v = 0 at 2.4 eV excitation energy from $B^2\Sigma+$ to $X^2\Sigma+$. The transitions from the lowest vibrational states correspond to high probability and strong relative intensity as compared to the highest vibrational states. The vibrational transitions associated with the spectrum emission lines of this CN molecular band were found at 388.34, 387.14, 386.19, 385.47, and 385.09 nm, respectively, along with the vibrational transitions (0,0), (1,1), (2,2), (3,3), and (4,4) at 3.2 eV excitation energy. Determining the concentration of nitrogen (N) and carbon (C) requires the detection of the CN band. The transitions between $d^3\Pi_g$ and $a^3\Pi_u$ can be seen in the C_2 Swan band system, commonly known as vibronic (400–700 nm), using the Plank equation (E = hc/λ). The C_2 optical emission's emission wavelength falls between the spectral range of 400 nm to 700 nm respectively. The C_2 swan band structure is at 467.3, (5,4), 468.3 (4,3), 469.8 (3,2), 471.6 (2,1), 473.7 (1,0), 509.6 (2,2), 512.9 (1,1), 516.5 (0,0), 550.2 (3,4), 554.1 (2,3), 558.5 (1,2), 563.5 (0,1), 600.5 (3,5), 606.0 (2,4), and 612.0 (1,3) nm are because of the transitions between $d^3\Pi_g$ and $a^3\Pi_u$ [35].

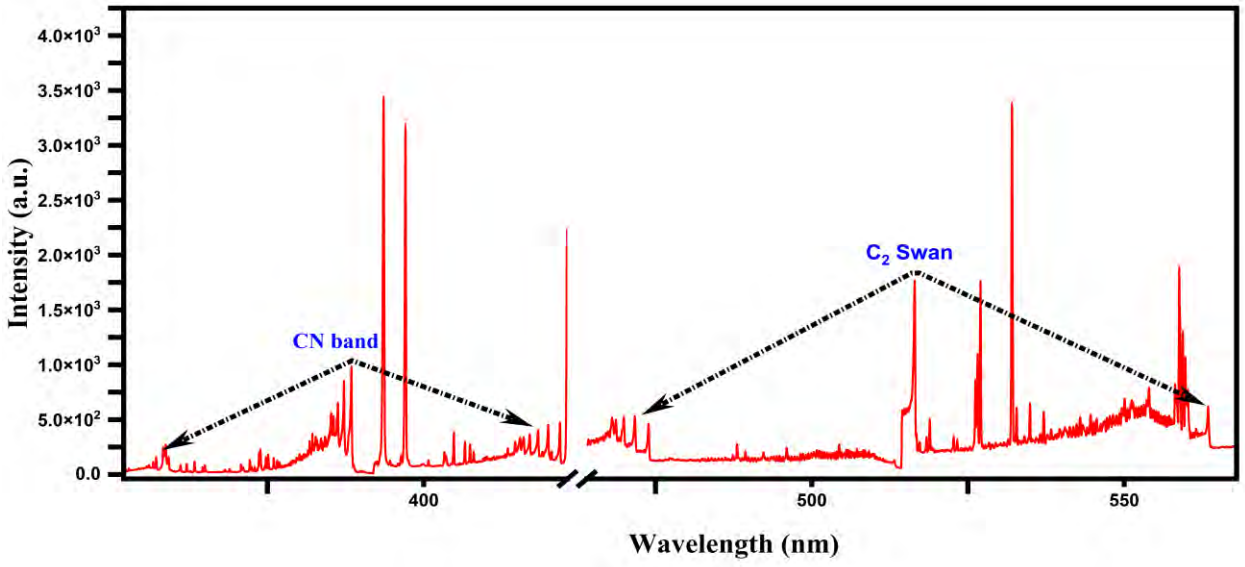

Figure 9 : Time-integrated spectrum of the DPM from 350nm to 565nm at different laser irradiance (GW/cm²) showing CN and C_2 vibrational optical spectrum

3.4 Electron Number Density:

The electron number density can be determined using the stark broadening width of particular lines in the spectrum that neutral atoms or ions emit. We select the interference-free spectral lines since they produce some appropriate results.

Since the plasma satisfies the requirements for thermodynamic equilibrium, we use stark broadening of the H_α line to measure the electron number density [36]. This is due to the fact that not all spectral lines are well-isolated lines have precise sharp broadening parameters. The lowest electron number density in local thermodynamic equilibrium is determined by a relation [37].

$$N_e \geq 1.6 \times 10^{12} \sqrt{T_k} (\Delta E_{ev})^3 \quad (3.1)$$

3.4.1 Stark broadening Method:

In our work, the electron number density in the plasma generated by the 532nm wavelength of the Nd: YAG laser is calculated by using the stark broadening parameter of the H_α line at 656.27 nm. The equation for calculating a spectral lines from full width half maximum (or stark broadening) is stated as by following equation, which represents stark broadening, is used to determine a spectral lines of full width half maxima (FWHM) [38].

$$\Delta\lambda_{1/2} = 2\omega\left(\frac{N_e}{10^{16}}\right) + 3.5A\omega\left(\frac{N_e}{10^{16}}\right)^{5/2} + \left[1 - \frac{3}{2}{N_D}^{-\frac{1}{3}}\right] \quad (3.2)$$

In this case, A, N_e and N_D stand for, respectively, electron impact parameter, ion broadening parameter, electron number density, and Debye sphere particles. The interaction between ions and atoms accounts for the second part in the equation above. Since the influence of the ion atom interaction is typically negligible, we may disregard it and use only one equation to determine the electron number density in cm^{-3} which is as follows:

$$N_e = 10^{17} \times \left(\frac{\Delta\lambda_{1/2}}{1.098}\right)^{1.47235} \quad (3.3)$$

The spectral lines shape profiles have Lorentzian characteristics. Figure-10 displays the Lorentzian-fitting H_α spectral line peaks obtained at 89mJ of Nd: YAG laser energy.

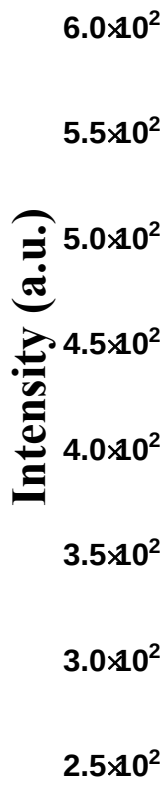

Figure 10 : Lorentzian fitting of spectral line 656.49 nm

By following the equation 3.3 we had calculated electron number density for SP LIBS spectrum by using FWHM of Hα line.

$$N_e = 10^{17} \times \left(\frac{\Delta\lambda_{1/2}}{1.098}\right)^{1.47235}$$

Where $\Delta\lambda_{1/2} = FWHM = 2.9$

$$N_e = 10^{17} \times \left(\frac{2.9}{1.098}\right)^{1.47235}$$

$$\boldsymbol{N_e = 2.54 \times 10^{17}\ cm^{-3}}$$

3.6 Local Thermodynamical Equilibrium (LTE) Condition:

For the optical plasma to be in local thermodynamic equilibrium (LTE), the ionic and excitation temperatures need to be similar to the electron temperature. In recent years, a number of tests have been created to verify the existence of thermodynamic equilibrium in a plasma. A minimal value of the electron density was proposed to ensure that collisions predominate the population of levels, which would demonstrate the existence or absence of thermodynamic equilibrium.

In order to confirm that the plasma is in LTE, McWhirter suggested using a foundation for a trivial limit of the electron number density [39].

$$N_e \geq 1.6 \times 10^{12} (\Delta E)^3 (T)^{1/2} \quad (3.4)$$

where T is the excitation temperature in kelvin (K) and E(eV) is the maximum transition energy from an upper to a lower ground level (n → m). **For measuring the LTE condition, we have select the line of Ca-I at 616.21 to check that the plasma is in LTE condition or not.**

Symbol	λ (nm)	T(K)	$T^{1/2}$	E(eV) (Lower)	E(eV) (Upper)	ΔE (eV)	$(\Delta E)^3$	$N_e \geq 1.6 \times 10^{12} (\Delta E)^3 (T)^{1/2}$
Ca-I	616.21	8700	93.27	1.89	3.91	2.02	8.13	1.23×10^{15}

Table 3 : illustrates the Ca-I at 616.21 for the LTE condition

The approximate electron number density of the sample is ($\mathbf{1.23 \times 10^{15}}$ **cm^{-3}**), using the temperature accordingly. This shows that the number density N_e ($\mathbf{2.54 \times 10^{17}\ cm^{-3}}$) calculated from stark

broadening lines is greater than the number density measured by using the Mc Whirter criterion. Therefore, it can be concluded that plasma is satisfying the LTE condition.

3.7 Optically Thin Plasma Condition:

In order to examine the laser-induced plasma spectroscopically, two parameters must be satisfied. The first is the LTE requirement, and the second is that the plasma had to be optically thin. We compare the theoretically line intensities with those calculated from the provided equation to determine if plasma is optically thin or not [16]:

$$\frac{I_1}{I_2} = \frac{A_1 g_1 \lambda_2}{A_2 g_2 \lambda_1} \times exp - \left(\frac{E_1 - E_2}{kT_e}\right) \quad (3.5)$$

Here, I_1 and I_2 stand in for the observed emission line intensities, while λ_1(nm) and λ_2(nm) are their wavelengths. The transition probabilities are represented by A_1 (s^{-1}) and A_2 (s^{-1}). g_1 and g_2 are the statistical weights and E_1 (eV) and E_2 (eV) represents the upper and lower energies of these observed transitions. To determine the intensity ratios, we used the sample's Ca-I emission lines at 428.93 nm and 429.89 nm. The right-hand side of this relation is the theoretical value uses the parameters catalogue in the NIST database.

Wavelength (nm)	**Element**	**Probability** $\boldsymbol{A \times 10^7}$	**E(ev)**	**g=2j+1**	$\boldsymbol{A_1 \times g_1 \times \lambda_2}$	$\boldsymbol{A_2 \times g_2 \times \lambda_1}$	$\boldsymbol{\frac{A_1 g_1 \lambda_2}{A_2 g_2 \lambda_1} \times exp - \left(\frac{E_1 - E_2}{kT_e}\right)}$
428.93	Ca-I	6×10^7	4.76	3	5983.44	7722	0.7748
429.89	Ca-I	4.66×10^7	4.76	3			

Table 4 : illustrates the optically thin plasma condition

Therefore, The RHS of the equation is theoretical value which is $\frac{I_1}{I_2} = \mathbf{0.7748.}$

The experimentally ratio of the intensities is $\frac{I_1}{I_2} = \mathbf{0.8296.}$

The experimental and theoretical intensity ratios for the sample is comparable with 7%.

3.8 Boltzmann plot for measuring Plasma Temperature:

The electron temperature of the plasma is calculated using the Boltzmann plot method, which is frequently used to analyse spectroscopic data. This method compares the relative intensities of two or more lines in the spectra with relatively large energy differences to determine the electron temperature of the plasma. To properly use the Boltzmann plot method to quantify T_e, the excitation level must be obtained in an LTE scenario. However, the Boltzmann plot equation that is used in the data analysis is:

$$\frac{N_j}{N_i} = \frac{g_j}{g_i} exp^{\frac{E_j - E_i}{kT_e}} \tag{3.3}$$

g_j and g_j represent the two levels' statistical weights.

K is the Boltzmann constant

T_e is the plasma temperature

$$\frac{N_j}{N_i} = \frac{g_j}{Z(T)} exp^{\frac{E_j}{kT_e}} \tag{3.4}$$

$Z(T)$ is the partition function

$$Z(T) = \sum_m g_m exp^{\frac{E_m}{kT_e}}$$

The emission intensity of this emission line can be expressed as a function of state.

$$I_{ji} = \frac{hc}{4\pi\lambda_{ji}} A_{ji} N_j \tag{3.5}$$

λ_{ji} is the emitted light's wavelength

h is Planck's constant

c is the vacuum speed of light

A_{ji} is the transition probability

By substituting this equation in eq 3.3 the resulting expression is

$$\frac{I_{ji}\lambda_{ji}}{g_i A_{ji}} = \frac{hCN}{4\pi Z(T)} exp^{\frac{E_j}{kT_e}} \quad (3.6)$$

By taking the logarithm on both side of the equation after we get.

$$ln\left(\frac{I_{ji}\lambda_{ji}}{g_i A_{ji}}\right) = -\frac{E_j}{kT_e} + C \quad (3.7)$$

Where C=$\ln(hcN/4\pi Z(T)$

which indicate a straight line equation. The slope of the straight line that is shown between energy and formula on the left side of equation 3.7 can be used to compute the electron temperature (T_e).

We will only pick the lines that are well separated/isolated, un-saturated, and spectrum at energy of 34.4mJ in order to determine plasma temperature. Table-5 lists the spectral lines' wavelengths and other pertinent information needed to determine the electron temperature.

Symbol	Wavelength	Statistical Weight g = 2J+1	Transition Probability A_{ji}	Intensity I	Energy of upper state cm^{-1}	$\frac{I_{ji}\lambda_{ji}}{g_i A_{ji}}$
Ca I	430.774	1	0.41438	800.46	38417.543	20.71917
Ca I	442.544	3	0.41762	738.02	37748.197	20.88079
Ca I	443.496	5	0.41643	1516.18	37751.867	20.82142
Ca I	504.162	3	0.41154	277.35	41679.008	20.57702
Ca I	527.027	5	0.425	1762.78	39340.08	21.24975
Ca I	612.222	3	0.43617	1167.56	31539.495	21.80873
Ca I	616.217	1	0.43152	1379.35	31539.495	21.57588
Ca I	646.257	7	0.42019	1338.93	35818.713	21.00936
Ca I	647.166	7	0.43471	476.88	35818.713	21.73554
Ca I	431.865	3	0.41143	720.28	38464.808	20.57147

Table 5 : illustrates the measured spectral lines for the Boltzmann plot

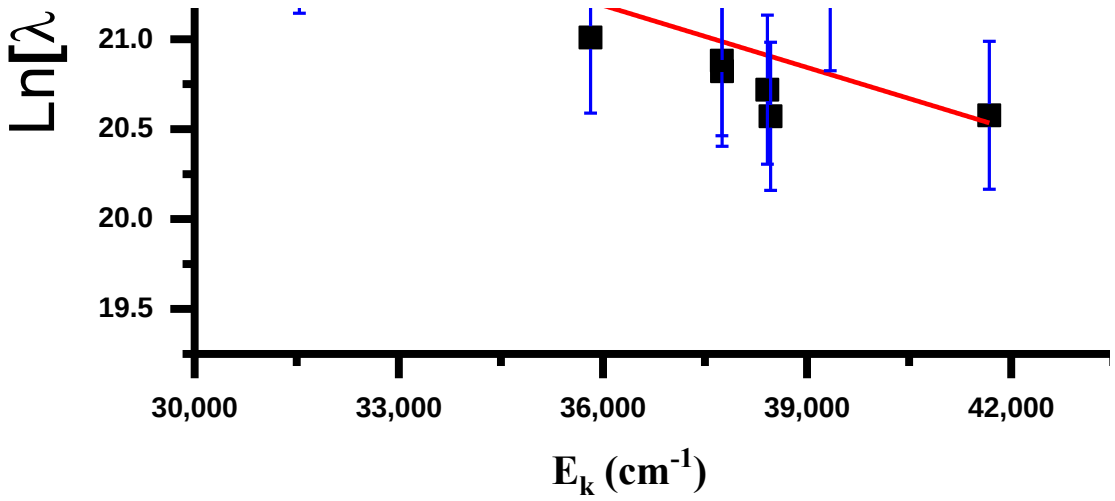

Figure 11 : Boltzmann plot of Ca-I spectral lines

Figure-11 illustrates the Boltzmann plot of the spectral lines of Ca-I shown in Table-5. The calculated plasma temperature of the LIBS spectrum is:

$$T_e = 8700 \pm 500 \text{ K}$$

3.9 Quantitative Analysis through Calibration Free Method:

The one-line calibration free (CF-LIBS) approach has been used to determine the composition of the elements for the Particulate matter sample by using the average values of electron densities and plasma temperatures in the Saha-Boltzmann equation [40]. The following Boltzmann equation was used to calculate the neutral atom concentration.

$$FC^z = I_k \frac{U^z(T)}{A_k g_k} e^{\frac{E_k}{kT}} \tag{3.8}$$

Where, F represent the ablated mass, C^z related to composition of the neutral atom, I_k related to the line intensity, g_k represent the statistical weight of the upper level transition; A_k related to the transition probability, $U^z(T)$ is the partition function, E_k is the upper level energy, T is the plasma temperature and K is the Boltzmann constant. The concentration of the ionized atoms C_{z+1} for the elements was measured by using the following Saha-Boltzmann equation [41].

$$n_e \frac{C^{z+1}}{C^z} = \frac{(2m_e kT)^{3/2}}{h^3} \frac{2U_{z+1}}{U_z} e^{-\frac{E_{ion}}{kT}} \ cm^{-3} \tag{3.9}$$

The amount of how much element is present in the sample is the sum of the neutral and ionic contributions.

$$C_T^a = C_z^a + C_{z+1}^a \tag{3.10}$$

The percentage composition of the element has calculated using the relationship:

$$C_{\%} = \frac{C_T^a}{C_T} \times 100 \tag{3.11}$$

where C_T^a represent the composition of each element and C_T represent the sum of the compositions of all of the elements present in the sample. The spectroscopic parameters of the spectral lines was selected to measure the concentrations was get from the NIST database ("NIST database" 2023). The results of how much concentration of elements are in the sample are listed in the table-6.

Fe %	Ca%	C%	Mg%	Li%	Na%	Ni%	H%	Cu%
89.86	4.76	4.06	0.13	0.03	0.06	0.93	0.13	0.01

Table 6 : shows the composition of all the elements in the DPM sample

Conclusion

In this study, a LIBS method for precise qualitative and quantitative analytical analyses of DPM is proposed. DPM sample was collected from diesel-powered passenger vehicle that was in used and came from well-known automaker. We discovered from LIBS analysis that DPM from in-use automobiles does not mostly contain pure carbon particles. Instead, it is mainly composed of several chemical elements in varying quantities. Major chemical elements in the DPM matrix can be measured instantaneously using the high-resolution LIBS approach. From qualitative LIBS measurements, we discovered the major DPM compounds: Carbon (C), Iron (Fe), Magnesium (Mg), Calcium (Ca) and Sodium (Na) elements. Instead major elements we have also discovered the trace and minor elements Lithium (Li), Copper (Cu) and Nickel (Ni). Special concern of this research has been given to the quantification analysis of the LIBS signal obtained from the different DPM matrix. We have characterised quantitatively the DPM sample and its main elemental compositions. Using a high-resolution LIBS approach.

we evaluated the qualitative and quantitative composition of the major chemical constituents in the DPM matrix in this work. However, further research will need to gather specific data on other significant elements present in DPM that could not be detected, specifically the amounts of sulphur and chlorine. The spectral window gap in our current LIBS configuration is to cause for this. Minor and trace components in DPM are of additional interest. Furthermore, we would like to compare the Particulate matter of diesel and petrol engines to check which elements are present in the patrol running vehicles. Having a general understanding of DPM and its chemistry can help in controlling combustion, diesel exhaust emissions, and diesel engines. Therefore, in the future, it will be essential to further aid in controlling and restricting undesirable pollutant emissions from diesel-engine driven vehicles in actual driving scenarios. This will be accomplished by developing the in situ LIBS technique for particulate matter. However, in addition to diesel fuel, fuel additives, and lubricating oils, after treatment devices like DPF, DOC, or catalytic converters can also have an impact on the ultimate PM emission composition from diesel-engine vehicles. As a result, it would be crucial to first evaluate specific parts and traces from these devices in order to understand and differentiate between the proportion of chemical elements and composition in the final PM matrix and the emissions from diesel engines. This information may be used in the future to comply with new emission standards and laws.

References

1. Wollaston, William Hyde (1802). "A method of examining refractive and dispersive powers, by prismatic reflection". Philosophical Transactions of the Royal Society of London. 92: 365– 380.
2. "A Timeline of Atomic Spectroscopy". Retrieved 24 November 2012.
3. R. M. Herd, MRCP(UK), J. S. Dover, and K. A. Arndt, "Basic Laser Principles," Dermatol. Clin., vol. 15, no. 3, pp. 355-372, 2005.
4. E. H. Evans, M. Horstwood, J. Pisonero, and C. M. M. Smith, "Atomic spectrometry update: Review of advances in atomic spectrometry and related techniques," J. Anal. At. Spectrom., vol. 28, no. 6, pp. 779-800, 2013.
5. N. H. Bings, A. Bogaerts, and A. C. Broekaert, "Atomic Spectroscopy A Review," vol. 82, no. 12, pp. 4653-4681, 2010.
6. W. Slavin and G. R. Carnrick, "Background Correction In Atomic Absorption Spectroscopy (Aas)," CRC Crit. Rev. Anal. Chem., vol. 19, no. 2, pp. 95-134, 1988.
7. V. A. Fassel, "Quantitative elemental analyses by plasma emission spectroscopy." Science (80-.)., vol. 202, no. 4364, p. 183, 1978.
8. J. R. Bacon, J. S. Crain, A. W. Mcmahon, and J. G. Williams, “Atomic mass spectrometry 1997," J. Anal. At. Spectrom., vol. 12, no. 10, pp. R407-R448, 1997.
9. F. J. Fortes, J. Moros, P. Lucena, L. M. Cabal, and J. J. Laserna, “Laser- Induced Breakdown Spectroscopy," 2013.
10. I.(Eds.). Miziolek, A., Palleschi, V., & Schechter, Laser Induced Breakdown Spectroscopy, vol. 14, no. 6. Elsevier Ltd, 2006.
11. K. Song, Y spectrometry. Appl., "Applications of laser-induced breakdown spectrometry," Appl. Spectrosc. Rev., vol. 32, no. 3, pp. 183- 235, 1997.
12. R. Noll et al., “Laser-induced breakdown spectroscopy expands into industrial applications," Spectrochim. Acta - Part B At. Spectrosc., vol. 93, pp. 41-51, 2014.
13. Q. I. Mohaidat, "Laser-induced breakdown spectroscopy (LIBS): An innovative tool for studying bacteria," Ph.D. thesis, 2011.
14. L. U. Claude and B. Lyon, "Characterization of laser-induced plasma and application to surface-assisted LIBS for powder and liquid samples.," 2018.

15. R. Gaudiuso, M. Dell'Aglio, O. de Pascale, G. S. Senesi, and A. de Giacomo, "Laser induced breakdown spectroscopy for elemental analysis in environmental, cultural heritage and space applications: A review of methods and results," Sensors, vol. 10, no. 8, pp. 7434-7468, 2010.
16. D. A. Rusak, B. C. Castle, B. W. Smith, and J. D. Winefordner, "Fundamentals and applications of laser-induced breakdown spectroscopy," Crit. Rev. Anal. Chem., vol. 27, no. 4, pp. 257-290, 1997.
17. D. W. Hahn and N. Omenetto, "Laser-induced breakdown spectroscopy (LIBS), part II: Review of instrumental and methodological approaches to material analysis and applications to different fields," Appl. Spectrosc., vol. 66, no. 4, pp. 347-419, 2012.
18. D. W. Hahn and N. Omenetto, "Laser-Induced Breakdown Spectroscopy (LIBS), Part I: Review of Basic Diagnostics and Plasma-Particle Interactions: Still-Challenging Issues within the Analytical Plasma Community," Appl. Spectrosc., vol. 64, no. 12, pp. 335A-336A, 2010.
19. Chen, Francis F. Introduction to plasma physics. Springer Science & Business Media, 2012.
20. Z. A. Umar, N. Ahmed, R. Ahmed, U. Liaqat, and M. A. Baig, "Elemental composition analysis of granite rocks using LIBS and LA- TOF-MS," Appl. Opt., vol. 57, no. 18, p. 4985, 2018.
21. J. El Haddad, L. Canioni, and B. Bousquet, "Good practices in LIBS analysis: Review and advices," Spectrochim. Acta Part B At. Spectrosc., vol. 101, pp. 171-182, 2014.
22. F. F. Chen, Introduction to Plasma Physics and Controlled Fusion. 2013.
23. J. Cooper, "Plasma spectroscopy Contents," Prog Phys, vol. 35, pp. 34- 130, 1966.
24. W. L.-H. (Ed.), Plasma Diagnostics. 1968.
25. S. L. L. (Eds.. R.W.P. McWhirter, Spectral intensities, in: R.H.Huddlestone, Plasma Diagnostic Techniques. Academic Press, 1965.
26. N. Ahmed, Z. A. Umar, R. Ahmed, and M. Aslam Baig, "On the elemental analysis of different cigarette brands using laser induced breakdown spectroscopy and laser-ablation time of flight mass spectrometry," Spectrochim. Acta - Part B At. Spectrosc., vol. 136, pp. 39-44, 2017.
27. C. J. Foot, Atomic Physics. Oxford University Press.
28. H. R. Griem and G. Peach, "Spectral Line Broadening by Plasmas," Phys. Today, vol. 28, no. 2, pp. 61-62, 1975.
29. H. R. Griem, Principles of Plasma Spectroscopy. Cambridge University Press, 1997.
30. A. Ciucci, M. Corsi, V. Palleschi, S. Rastelli, A. Salvetti, and E. Tognoni, "New procedure for quantitative elemental analysis by laser- induced plasma spectroscopy," Appl. Spectrosc., vol. 53, no. 8, pp. 960- 964, 1999.

31. E. Tognoni et al., “A numerical study of expected accuracy and precision in Calibration-Free Laser-Induced Breakdown Spectroscopy in the assumption of ideal analytical plasma," Spectrochim. Acta - Part B At. Spectrosc., vol. 62, no. 12, pp. 1287-1302, 2007.
32. E. Tognoni, G. Cristoforetti, S. Legnaioli, and V. Palleschi, "Calibration-Free Laser-Induced Breakdown Spectroscopy: State of the art," Spectrochim. Acta - Part B At. Spectrosc., vol. 65, no. 1, pp. 1-14, 2010.
33. J. D. Pedarnig, P. Kolmhofer, N. Huber, B. Praher, J. Heitz, and R. Rössler, "Element analysis of complex materials by calibration-free laser-induced breakdown spectroscopy," Appl. Phys. A Mater. Sci. Process., vol. 112, no. 1, pp. 105-111, 2013.
34. Shortland, A.J., Application of lead isotope analysis to a wide range of Late Bronze Age Egyptian materials. Archaeometry, 2006. 48(4): p. 657-669.
35. Alrebdi, Tahani A., Amir Fayyaz, Amira Ben Gouider Trabelsi, Haroon Asghar, Fatemah H. Alkallas, and Ali M. Alshehri. "Vibrational Emission Study of the CN and C2 in Nylon and ZnO/Nylon Polymer Using Laser-Induced Breakdown Spectroscopy (LIBS)." *Polymers* 14, no. 17 (2022): 3686.
36. El-Rabii, Hazem, Sergey B. Victorov, and Azer P. Yalin. "Properties of an air plasma generated by ultraviolet nanosecond laser pulses." *Journal of Physics D: Applied Physics* 42, no. 7 (2009): 075203.
37. Fujimoto, Takashi, and R. W. P. McWhirter. "Validity criteria for local thermodynamic equilibrium in plasma spectroscopy." *Physical Review A* 42, no. 11 (1990): 6588.
38. Ashkenazy, J., R. Kipper, and M. Caner. "Spectroscopic measurements of electron density of capillary plasma based on Stark broadening of hydrogen lines." *Physical Review A* 43, no. 10 (1991): 5568.
39. (McWhirter 1965; Konjevic et al. 2002; Harilal et al. 2005; Cristoforetti et al. 2010; Unnikrishnan et al. 2012
40. Ciucci et al. 1999; Togoni et al. 2007; Umar et al. 2018
41. Pandhija and Rai 2009; Takahashi et al. 2015